Journal of Non-Newtonian Fluid Mechanics 194 (2013) 1–13

Contents lists available at SciVerse ScienceDirect

Journal of Non-Newtonian Fluid Mechanics

journal homepage: http://www.elsevier.com/locate/jnnfm

The formation of vortex rings in shear-thinning liquids

Carlos Palacios-Morales [a], Roberto Zenit [b,*]

[a] Departamento de Termofluidos, Facultad de Ingeniería, Universidad Nacional Autónoma de México, Av. Universidad 3000, México D.F. 04510, Mexico
[b] Instituto de Investigaciones en Materiales, Universidad Nacional Autónoma de México, Apdo. 70-360, México D.F. 04510, Mexico

ARTICLE INFO

Article history:
Received 1 June 2012
Received in revised form 26 September 2012
Accepted 5 November 2012
Available online 3 December 2012

Keywords:
Vortex rings
Non-Newtonian
Shear-thinning liquids

ABSTRACT

The dynamics of formation and evolution of vortex rings in non-Newtonian shear-thinning liquids generated in a piston-cylinder arrangement was studied. The ratio of the piston displacement L_m to the internal cylinder diameter D_0, as well as the mean piston velocity U_p determine the vortex properties and evolution. Experiments with different conditions are presented: translation velocity of the piston and stroke ratios L_m/D_0. Measurements of the 2D velocity field were obtained with a PIV technique. The vortex circulation Γ was computed considering a vortex identification scheme (Q criterion). The Reynolds number was in the range $138 < Re_0 < 616$. The Reynolds number for these vortices was computed in terms of the 'power-law' model parameters: the power index n and the consistency m. Considering different shear-thinning liquids and fixed Reynolds number, we observed that the vortex circulation decreases with the power index n. We show that the total circulation ejected from the cylinder is reduced when the thinning property of the liquid increases (decrease n); thus, the circulation confined inside the vortex ring, is reduced too. A value of the non-dimensional vortex circulation $\Gamma/D_0U_p \approx 2$ may indicate a saturation condition beyond which it is not possible to increase the vortex circulation for any Reynolds number.

1. Introduction

Vortex rings are fundamentally important in fluid mechanics due to their prevalence in a variety of flows including turbulence. Vortex rings are present in many engineering applications and natural phenomena. Some examples are starting jets, helicopter rotors, propulsion, volcanic eruptions, animal locomotion, etc. A great volume of research in this subject has been published for over a century. The vortex ring is one of the most common fluid structures in nature. Many biological flows are characterized by vortex production and vortex shedding. In animal locomotion, the production of coherent structures such as vortex rings is common; these structures have been found in squid jet propulsion by Anderson and Grosenbaugh [1] and Bartol et al. [2]. Dabiri et al. [3] studied a species of jellyfish that creates a single vortex ring. This kind of vortex can also be seen in internal biological flows, such like the discharge of blood into the heart left ventricle (Gharib et al. [4]).

In the laboratory, vortex rings can be generated by the motion of a piston that pushes a column of fluid in a cylinder through an orifice or nozzle. In the literature it is possible to find theoretical, numerical and experimental studies that address this problem. Many of the early works can be found in the reviews of Shariff and Leonard [5] and Lim and Nickels [6]. Saffman [7] presented different theoretical studies of axisymmetric thin cored vortex rings. There are many experimental studies for the case of laminar vortex rings in Newtonian fluids: Maxworthy [8] observed that the vortex formation process is strongly dependent on Reynolds number. Didden [9] gave information of the role of the internal and external boundary layers in the formation process and circulation of the vortex ring. Glezeer [10] analyzed the conditions under which transition from laminar to turbulent vortex rings is observed. Weigand and Gharib [11] studied the vortex ring properties for different Reynolds numbers using the PIV technique and found that the vorticity distributions in the vortex core have self-similar Gaussian profiles. Gharib et al. [12] reported that for large piston displacements the vortex rings attain a maximum circulation during their formation. Querzoli et al. [13] studied experimentally the motion of vortex rings generated by gradually varied flows which reproduce the characteristics of many biological conditions. Palacios-Morales and Zenit [14] studied the vortex ring formation for relatively low Reynolds numbers. Rosenfeld et al. [15] used the Navier–Stokes equation to simulate the vortex ring formation and evolution for relatively long discharge times (long displacement of the piston) and compared their numerical results with the Gharib et al. [12] experiments. Mohseni et al. [16] simulated the formation of vortex rings that are generated by applying a non-conservative force of long duration.

* Corresponding author. Tel.: +52 55 5622 4593; fax: +52 55 5622 4602.
E-mail addresses: palacios.ca@gmail.com (C. Palacios-Morales), zenit@unam.mx (R. Zenit).

0377-0257/$ - see front matter © 2012 Elsevier B.V. All rights reserved.
http://dx.doi.org/10.1016/j.jnnfm.2012.11.002

It is important to highlight that all studies about vortex rings have been conducted in Newtonian fluids; however, many fluids in nature and in many industrial applications have non-Newtonian characteristics. To our knowledge the motion of annular vortices has not been studied to date for the case of a non-Newtonian fluid. The understanding of this subject could have influence of other related subjects. For instance, Coelho and Pinho [17,18] studied the vortex shedding behind a cylinder in cross-flow for the case of shear thinning viscoelastic flows. They attributed an increase of the dimensionless vortex shedding frequency to shear thinning effects. As we will explain later, the increment of vortex shedding frequency could be attributed to the reduced circulation that can be attained by vortices in shear thinning fluids. In a different study, Bohome and coworkers [19] studied the vortex breakdown of torsionally driven cavities for shear thinning fluids. They found that, as a result of the thinning nature of the fluid, the critical Reynolds number for which the breakdown is observed is reduced. Again, such observation is in qualitative agreement with the present results: vortices in shear thinning fluid cannot contain as much vorticity in their core; hence, the breakdown occurs sooner.

In particular we are interested in the study of vortex ring formation using blood-like liquids. Vortex rings are generated inside the human heart at the left ventricle when blood is discharged during cardiac diastole. It has been shown by [4] that the optimal ring formation might be an indicator of cardiac health. To date, it is not possible to predict what is the influence of non-Newtonian fluid properties in the formation process of vortex rings. In this investigation, we conducted an experimental study to provide some insight into this subject. To simplify the problem as much as possible, we considered only shear-thinning fluids. In particular we determined the influence of the thinning properties on the maximum circulation that a single vortex can attain.

1.1. Background

For the piston-cylinder arrangement, the parameter L/D_0, also called 'stroke ratio', determines many properties of the vortex rings. $L = L(t)$ is the piston displacement and D_0 is the inner diameter of the cylinder exit. The stroke ratio is equivalent to the non-dimensional time

$$t^* = \frac{\overline{U_p}t}{D_0} = \frac{L}{D_0} \tag{1}$$

referred as the *formation time* by Gharib et al. [12]. $\overline{U_p}$ is the mean piston velocity during fluid discharge and t is the discharge time. The "total stroke ratio" is equivalent to the total non-dimensional time

$$T^* = \frac{\overline{U_p}T_0}{D_0} = \frac{L_m}{D_0} \tag{2}$$

where L_m is the total piston displacement and T_0 is the total discharge time. For Newtonian vortex rings Gharib et al. [12] found that for values smaller than $L_m/D_0 \approx 4$, a solitary vortex ring was formed; for larger values of L_m/D_0, a leading vortex followed by a trailing jet and secondary vortices were observed. They also reported that the circulation contained within the leading vortex ring could not be further increased for $L_m/D_0 \geqslant 4$.

The 'slug model' considers that the vortex ring is generated by a cylindrical 'slug' of fluid that is ejected from a nozzle using a piston-cylinder arrangement [6]. The model considers that the boundary layer thickness $\beta \ll D_0/2$ and the wall-normal velocity component u_r is much smaller than the streamwise component u_x. Under these conditions, the change in circulation can be written as:

$$\frac{d\Gamma}{dt} \approx \int_{D/2-\beta}^{D/2} \omega_\phi u_x \, dr \approx \int_{D/2-\beta}^{D/2} u_x \left(-\frac{du_x}{dr}\right) dr \tag{3}$$

where ω_ϕ is the vorticity in the azimuthal direction. Considering that the velocity at the edge of the boundary layer is equal to the piston velocity U_p, the total circulation ejected through the cylinder exit is expressed as

$$\Gamma_{slug} \approx \int_0^{T_0} \left[-\frac{u_x^2}{2}\right]_{D/2-\beta}^{D/2} dt = \frac{1}{2}U_p^2 T_0 = \frac{1}{2}U_p L_m. \tag{4}$$

Previous investigations have found some differences between the slug model and the actual experimental results; the discrepancies have been attributed to different causes [9]. Nevertheless, the slug model has been used by many authors to derive analytical and empirical models (inviscid and viscous) to predict some vortex ring properties as the translation velocity, size and the vortex circulation [13,20,21].

The experimental results of Gharib et al. [12] and others indicate that for large stroke ratios, the vortex ring separates from its trailing jet (pinch-off process) at a finite formation time t^*. In other words, the vorticity field of the leading vortex ring disconnects from that of the trailing jet. However, for relatively low Reynolds numbers this separation does not occur or is not noticeable as discussed in depth by [2]. For this reason, in this investigation, the Q criterion [22] is used to identify the vortex core region. For two dimensional flows, the Q criterion is also known as the *Okubo-Weiss* criterion [23,24]. The second invariant Q, for an incompressible flow ($\nabla \cdot \boldsymbol{u} = 0$) is defined as

$$Q = \frac{1}{2}(|\boldsymbol{\Omega}|^2 - |\boldsymbol{D}|^2) \tag{5}$$

where $\boldsymbol{D}$ is the symmetric (rate of strain tensor) and $\boldsymbol{\Omega}$ the antisymmetric (vorticity tensor) components of the velocity gradient tensor $\nabla\boldsymbol{u}$, respectively. The norm of the tensors is defined as $|\boldsymbol{\Omega}| = tr[\boldsymbol{\Omega}\boldsymbol{\Omega}^t]^{1/2}$ and $|\boldsymbol{D}| = tr[\boldsymbol{D}\boldsymbol{D}^t]^{1/2}$. With this technique we can find flow regions ($Q > 0$) where the vorticity magnitude (solid-body rotation of the fluid) prevails over the strain-rate magnitude (deformation of the fluid); therefore, it is possible to obtain closed areas to integrate the vorticity and compute the vortex ring circulation.

Some authors have used stream lines or peak vorticity values to find the vortex centers [12,13]. We used a method to find topologically relevant points in the flow [25] to locate the vortex ring center. In a two-dimensional flow, special points can be found in the regions where the local velocity becomes zero. When located in a region of the flow where the vorticity dominates, such points are elliptic; in a strain-dominated region, they are hyperbolic (i.e., saddlelike). It has been shown that the elliptical points correspond to the geometric centers of the vortices in the flow [26]. It is possible to find the elliptic and hyperbolic points by computing the curvature of Lagrangian trajectories, that is, the trajectories of individual moving fluid elements; in this investigation, we use the 2D velocity field obtained by the PIV technique. Near both hyperbolic and elliptic points, the direction of fluid particle trajectories changes over very short length scales, producing large curvature values. The curvature was obtained following the scheme of Braun et al. [27]:

$$k(t) = \frac{|\boldsymbol{u} \times \partial_t \boldsymbol{u} + \boldsymbol{u} \times [\boldsymbol{u} \cdot \nabla \boldsymbol{u}]|}{|\boldsymbol{u}|^3} \tag{6}$$

where $\boldsymbol{u}$ is the velocity field and ∂_t is the partial time derivative. Once the points of local maximum curvature are identified, it is possible to classify them as elliptic or hyperbolic using the Q criterion described above. If the special point has a Q value $Q > 0$, where rotation dominates, the point is the center of a vortex. The term

$\boldsymbol{u} \times \partial_t \boldsymbol{u}$ is obtained using a central difference computation of three successive vector maps. The time resolution of our experiments (15 Hz) is sufficient to compute the temporal term; however, it is also possible to compute the curvature without this term obtaining differences (peak curvature position) lower than 0.8% in the axial direction.

In general, the Newtonian constitutive equation accurately describes the rheological behavior of low molecular weight liquids and some polymers at very slow rates of deformation. Many models that depend on the rate of deformation arise from the so called 'generalized Newtonian model'. The most common is the *power law model* [28]:

$$\eta = m\left[\sqrt{\frac{1}{2}(\dot{\gamma} : \dot{\gamma})}\right]^{n-1} \tag{7}$$

where n and m are the power-law index and the 'consistency', respectively. $\eta = \eta(\dot{\gamma})$ is commonly known as the apparent fluid viscosity and $\dot{\gamma}$ is the shear rate tensor. For $n = 1$ the Newtonian case is recovered. The power law model is a good approximation for the behavior of many polymeric liquids and dispersions. In particular for shear-thinning fluids, for which $n < 1$, at high shear rate ($\dot{\gamma} > 1\ s^{-1}$), the power law fits experimental data well. This model has also been used to model shear thickening fluids, for which $n > 1$. One of the disadvantages of the power law is that it fails to describe the low shear rate region in which η goes to infinity rather than to a constant η_0. For a more realistic description of flow, the Carreau–Yasuda model is used [28]. To avoid ambiguity, we have defined the Reynolds number in terms of the *power law* model parameters. Considering a characteristic shear rate $\dot{\gamma} \approx 2U_p/D_0$ and $\eta \approx m\dot{\gamma}^{n-1}$ the Reynolds number is defined as

$$Re_0 = \frac{2^{1-n}\rho U_p^{2-n} D_0^n}{m} \tag{8}$$

where ρ is the density of the fluid. For Newtonian liquids $n = 1$ and $m = \mu$ (liquid dynamic viscosity); therefore, $Re_0 = \rho U_p D_0/\mu$ which is the definition of the Reynolds number for Newtonian vortex rings used by some authors [8,9,15]. Note that this rheological model does not account for viscoelastic effects. In this investigation the liquids that were used, were prepared such that viscoelastic effects were not presented or at the very least, had a negligible effect.

2. Experimental setup

The experimental setup is shown in Fig. 1. Vortex rings were generated in a tank using a piston-cylinder arrangement. The cylinder is submerged in liquid with a free surface. The tank dimensions are: $20 \times 18 \times 40$ cm. The cylinder is 40 cm long and its inner diameter is $D_0 = 19.4$ mm. The nozzle exit is placed $\sim 3.6D_0$ from the back wall (BW), $\sim 6.4D_0$ from the lateral walls (LWs) and $\sim 17D_0$ from the frontal wall (FW). The axial axis x is placed to coincide with the center-line of the cylinder ($r = 0$) and the nozzle exit plane is located in the plane $x = 0$. A sharp-edged cylindrical nozzle was coupled at the end of the cylinder. The tip angle of the nozzle is $\theta_{noz} = 20°$ and the exit diameter is also 19.4 mm. This angle avoids wall effects at the exit on the formed vortex rings.

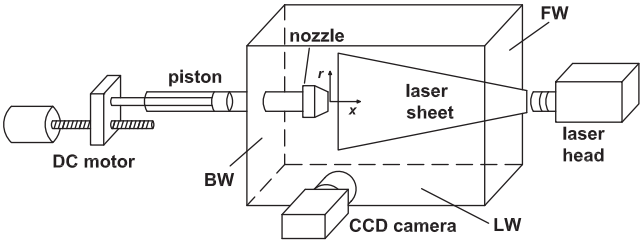

Fig. 1. Experimental setup.

The piston is coupled to a driving mechanism which is moved, in turn, by a DC motor with maximum output velocity of 1700 rpm. The DC motor is fed by a power supply which is controlled by a computer such that it is possible to control and fix the piston velocity and displacement. Specifically, we controlled the piston velocity program by varying the voltage and duration of supply. The mean piston velocity U_p was proportional to the supplied voltage. If the desired displacement was $L_m = jD_0$, where $j = 1, 2, \ldots, 10$, the piston moved a distance x_p so $|x_p - L_m|/L_m \leqslant 0.02$. All the piston velocity programs were *impulsive* and the mean piston velocity was reached at 0.25 s approximately. The maximum piston velocity was $U_p = 20$ cm/s.

Two dimensional velocity fields were obtained using the particle image velocimetry (PIV) technique. A Nd:YAG laser system generates a 50 mJ energy 532 nm laser beam which was converted to a laser sheet using a cylindrical lens. The laser sheet illuminates a vertical slice of the tank at the center of the cylinder. A CCD camera is placed perpendicular to the laser sheet. The camera records images with a resolution of 1008×1016 pixels. For most of the experiments the typical measurement area was 152×153 mm^2. Silver-coated hollow glass spheres with an average diameter 10 ± 5 μm were used as particle tracers. The velocity field consisted of 62×62 vectors using an interrogation area of 32×32 pixels and an overlap of 50%. The sampling rate was 15 Hz. A detailed description of the PIV technique can be found in [29,30]. To calculate vorticity and curvature scalar maps (and also peak values) we first constructed a subgrid of $\Delta x/3$ and $\Delta y/3$ ($\sim$0.75 mm) nodes, then the velocity field is interpolated to fit the subgrid using triangle-based linear interpolation.

2.1. Test liquids

In the present work we used different aqueous solutions of xanthan gum. This gum is produced by fermentation of glucose or sucrose and is used as food additive and rheology modifier. The viscosity of xanthan gum solutions increases with concentration and decreases with shear rate (shear-thinning behavior). The addition of xanthan gum to glycerol solutions and also diluted potassium thiocyanate solutions, has been used to produce transparent blood-like fluids [31]. For all experiments we used a KELTROL® (distributed by CPkelco) xanthan gum which is used for food and personal care applications. To prepare the solutions, we first dissolved the xanthan gum in water (at 55 °C) and left them to rest for 24 h before experiments. In order to compare with a Newtonian liquid, a glycerol solution was also used. Table 1 presents all physical properties of the different solutions used in the present investigation. For the shear thinning liquids, the increasing number in the nomenclature indicates a more pronounced shear thinning effect. Note that we choose the liquids and the conditions of the experiments that match the Reynolds number. In this manner we can isolate the effect of the thinning property.

In Fig. 2 we present the viscosity as a function of the shear rate $\dot{\gamma}$ for different xanthan solutions. Viscosity measurements were obtained using a stress-control Rheometer AR 1000-N from T.A. Instruments ®. We used a cone-plate geometry with 60 mm diameter, 2° angle and gap equal to 65 μm. All measurements were performed at a temperature of 23 °C. Liquid viscosities were obtained for shear strain rates in between $1 \leqslant \dot{\gamma} \leqslant 200\ s^{-1}$. Different levels of shear stress were applied to improve the measurement, particularly for the cases of small shear rates. With this instrument we also monitored the value of the first normal stress difference to detect possible viscoelastic effects. In all cases the normal stress was negligible or too small. To measure the Newtonian liquid viscosity we used the Brookfield ®DV-III viscometer. The plotted lines in

Table 1
Physical properties of the test liquids. The number after liquid represents parts per million. For the case of glycerin the number represent the percentage in weight of glycerin in water.

Liquid		Density (kg/m^3)	Consistency m (mPa s^n)	Power index n	Re_0
ST1	Xan-450	1000	23.5	0.6088	138
	Xan-450	1000	"	"	265
	Xan-450	1000	"	"	616
ST2	Xan-600	1000	41.5	0.5431	261.8
ST3	Xan-900	1000	88.9	0.4781	262
N	Gly-65	1151	μ = 13.59	1	263

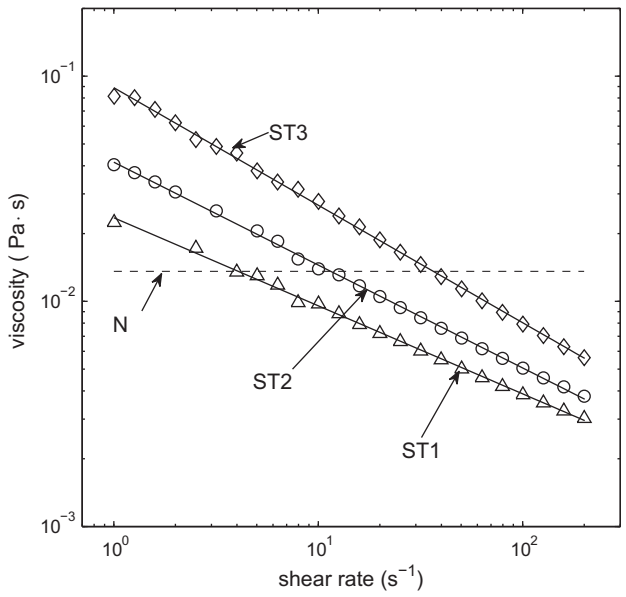

Fig. 2. Viscosity as function of shear rate for different xanthan solutions.

Fig. 2 correspond to the power law model $\eta = m\dot{\gamma}^{n-1}$; where m and n are shown in Table 1 for each liquid. We can observe that this model fits well experimental data for the measured shear rate range. The shear rates observed in the flow during the formation of vortices are within this range of shear rates. We also conducted oscillatory tests (as those of Vélez-Cordero et al. [32]) to further show that the elastic effects were small. However, the oscillatory and shear flow tests did not show any measurable evidence of elasticity, i.e. these effects are too small to be measurable with our apparatus. The typical relaxation time, λ, for diluted polymeric solutions such as those used in the present investigation is of the order O(10^{-5} s) which is much smaller than the characteristic time for all cases; this indicates that the elastic effects are indeed negligible. In other words, the Weissenberg number $We = 2\lambda U_p/D_0$ is of order O(10^{-3}) for all cases.

3. Results

3.1. Vortex ring image maps

In Figs. 3 and 4, we present the image maps of two shear-thinning vortex rings with the same Reynolds number but different stroke ratio. The image maps are: (a) velocity field, (b) vorticity field (s^{-1}), (c) stream line field, (d) velocity magnitude (m/s), (e) Q criterion (s^{-2}), and (f) the local strain (s^{-1}). Fig. 3 shows a vortex ring generated in the ST1 fluid with stroke ratio $L_m/D_0 = 4$ and $Re_0 = 265$. In this case we observe an isolated vortex ring located at a distance $x \approx 4D_0$ (considering maximum point of curvature). Compared with higher Reynolds numbers [12], the vortex rings with $Re_0 \sim$ O(100) tend to broaden in the axial direction, which can be observed in the vorticity field (Fig. 3b). The center of the vortex ring in the vector field coincides well with the vortex center in the stream lines map ($r/D_0 \approx 1$); however, the vorticity peak tends to move towards the axis of symmetry where velocity gradients are higher, as observed by [14]. The Q criterion map shows the regions where the fluid rotation dominates which correspond to the vortex ring core. Finally Fig. 3e shows the local strain of the flow obtained by computing the norm of the 'strain tensor' $|\boldsymbol{D}|$. We observe that the largest strain occurs in front of the vortex ring.

Fig. 4 shows the image maps for a vortex ring formed with the same liquid and Reynolds number as the previous case but with stroke ratio $L_m/D_0 = 8$. In this case we observe that the vortex ring is connected with a trailing jet flow. As mentioned above, for such small Reynolds numbers, a physical separation between both regions never occurs. In Fig. 4b we observe zones of large vorticity in both the leading vortex and the trailing jet. High strain values (Fig. 4e) appear in front of the leading vortex as well as the trailing jet where there are high velocity gradients. We observe that for all cases the maximum local strain rate values are of O(10) s^{-1} (for example, 5.8 s^{-1} in Fig. 4f). In Fig. 2, it was shown that for $10 < \dot{\gamma} < 10^2$ s^{-1}, all fluids showed shear thinning behavior. Therefore, we are certain that at the first stages of formation the non-Newtonian properties affect the dynamic of the vortex. As the vortex velocity decreases, the local strain decreases too and the liquid behaves more as a viscous Newtonian fluid. Several authors [12,14,15] have studied the transition between vortex rings with and without a trailing jet flow for Newtonian fluids. For different experimental conditions the critical stroke ratio for which the trailing jet appears is $L_m/D_0 \approx 4$ which agree with our experimental observations for non-Newtonian vortex rings.

Measurements obtained for the Newtonian liquid show the same qualitative features as those shown in Figs. 3 and 4 for the shear thinning fluid. In most cases, no significant variations can be observed from simple visual inspection. However, we can observe some qualitative differences in Fig. 5, where we present, for the same Re_0 and stroke ratio, the vector and vorticity fields for the Newtonian and the most shear-thinning liquid (ST3). Vortex centers are located at $x \approx 4D_0$. First, we observe that the axial velocity profile u_x is parabolic at the nozzle exit for the Newtonian liquid (Fig. 5a); while a more plug-like velocity profile is observed for the ST3 fluid (Fig. 5b). Consider that, in both cases, the piston was still moving at the time these pictures were taken. These profile differences in the axial direction are further discussed in this paper. The vorticity fields show a particular difference in the trailing jet behavior. We observe two different vorticity regions for the Newtonian liquid, one for the vortex ring and another for the trailing jet. Instead, for the ST3 fluid, we observe a single vorticity region for both the vortex ring and the jet. This vorticity distribution has not been observed for Newtonian fluids with low Re_0 in the present investigation and previous investigations [14].

3.2. Vortex ring properties

For the following results (vortex properties and vortex circulation), two different comparisons are presented. In cases (a), we

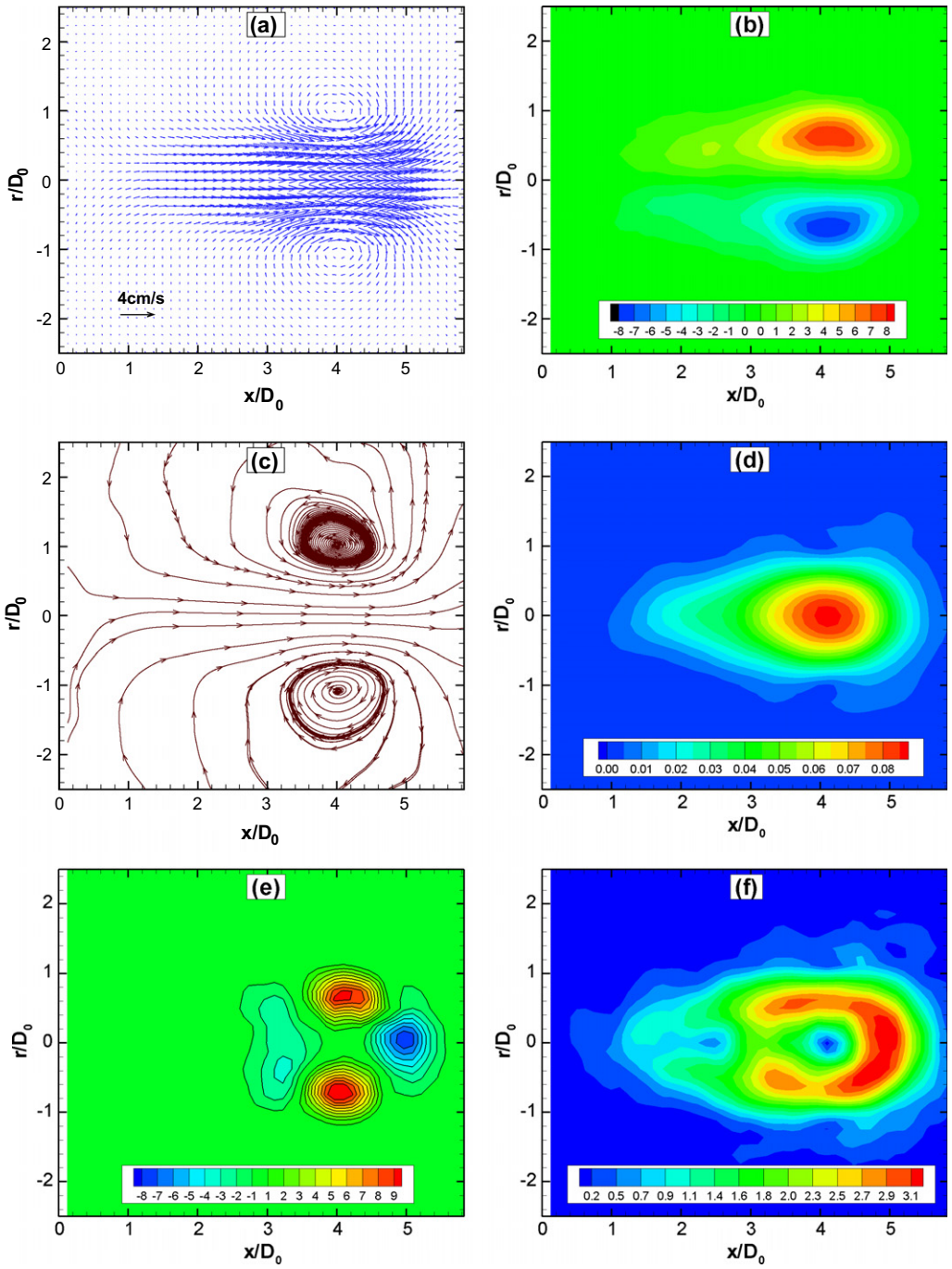

Fig. 3. ST1 fluid $L_m/D_0 = 4$ $Re_0 = 265$ $x \approx 4D_0$. (a) velocity field, (b) vorticity (s^{-1}), (c) stream lines, (d) velocity magnitude (m/s), (e) Q criterion (s^{-2}), and (f) local strain (s^{-1}).

evaluate the effect of inertia (Reynolds number) or the stroke ratio L_m/D_0 for a given shear-thinning fluid; in cases (b) we evaluate the shear-thinning nature (n) of different liquids for the same Reynolds number.

In Fig. 6 we show the trajectories of the vortex rings: (a) ST1 fluid with different Reynolds numbers and a stroke ratio of $L_m/D_0 = 4$, (b) All liquids for $Re_0 \approx 260$ and $L_m/D_0 = 4$. Each data series represents the trajectory of a single vortex ring; the center position of the upper vortex ring section ($r > 0$) is presented considering maximum curvature. In Fig. 6a we observe that the initial position of the vortex ring with $Re_0 = 138$ is $r \approx 0.8D_0$; just after four diameters of travel in the axial direction, the vortex ceases its motion in this direction and begins to expand radially, i.e the vortex ring diameter increases. The initial position of the vortex for $Re_0 = 265$ and $Re_0 = 616$ is in the range $0.9 \leqslant r/D_0 \leqslant 1$, which is slightly higher than the first case; however, in the same way, the vortex ring slows down in the axial radiation and begins to grow radially before it dissipates completely. In Fig. 6b we observe that the initial position for all cases is close to $r = D_0$ and a sudden expansion in the radial direction is presented for all shear-thinning vortices. We observe that as we increase the thinning nature of the fluid (decreasing n), the vortex ring stops its motion at a smaller distance from the exit nozzle. For the Newtonian case, we observe a more gradual increase of the vortex radius along the seven diameters presented

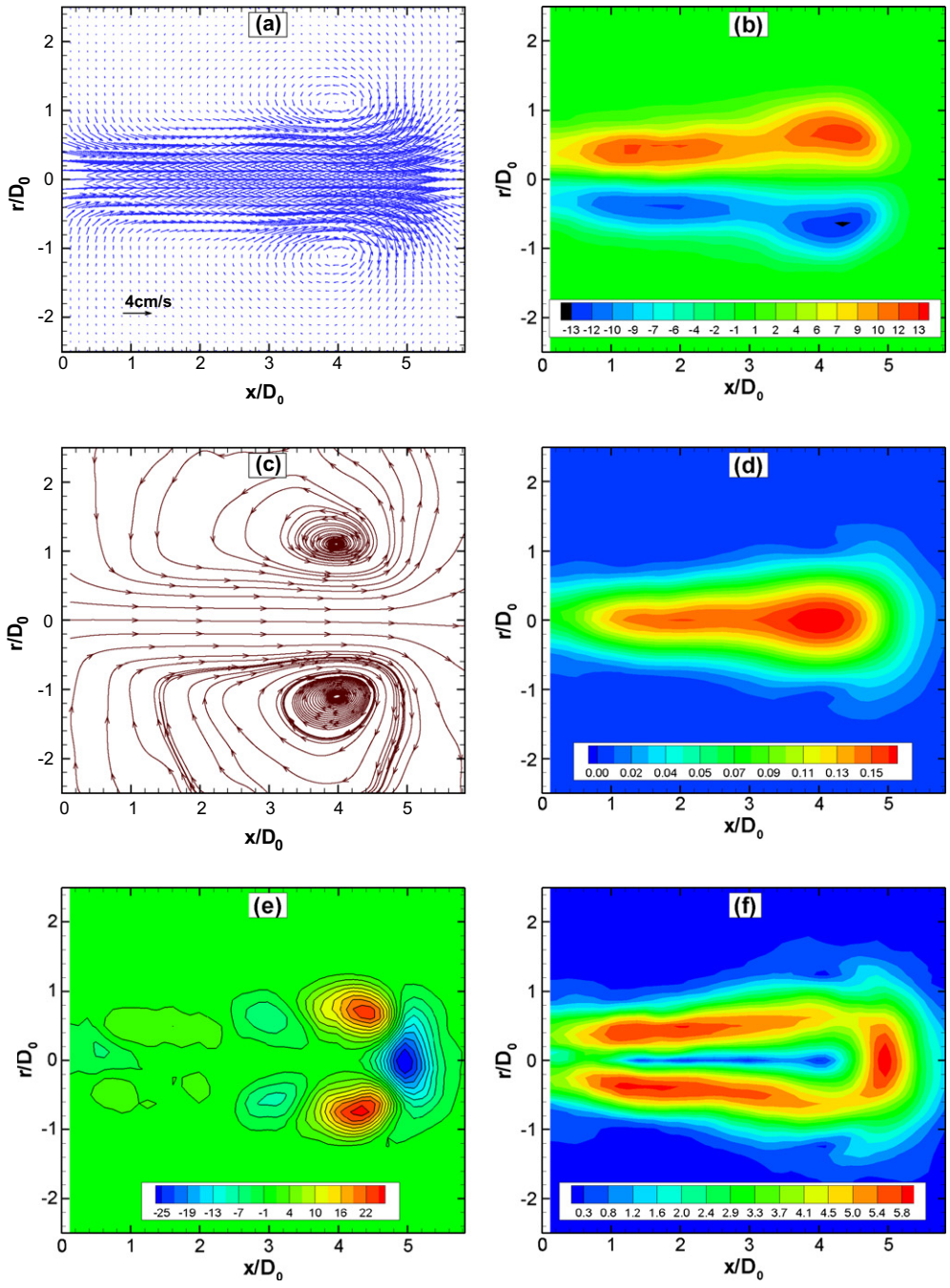

Fig. 4. ST1 fluid $L_m/D_0 = 8$ $Re_0 = 265$ $x \approx 4D_0$. (a) velocity field, (b) vorticity (s^{-1}), (c) stream lines, (d) velocity magnitude (m/s), (e) Q criterion (s^{-2}), and (f) local strain (s^{-1}).

in the figure. To our knowledge, this sudden change in the vortex radius is not presented in Newtonian vortex rings regardless the Reynolds numbers.

Fig. 7 shows the non-dimensional vortex ring diameter D_v/D_0 for the ST1 fluid with $Re_0 = 265$ and different stroke ratios. Similarly as above, each data series exhibits the evolution (diameter) of a single vortex ring. x_m is the mean x-position of the vortex centers, i.e. the upper and lower vortex ring sections. First, we observe that the initial vortex diameter is in the range $1.8 \leqslant D_v/D_0 \leqslant 2$. For small stroke ratios ($L/D < 4$) the vortex ring stops its motion close to the nozzle; for example, when $L_m/D_0 = 2$ the vortex stops at approximately $3D_0$. For larger L_m/D_0 the ring diameter increases as the vortex moves away from the exit nozzle. Didden [9] reported that the vortex (Newtonian) diameter increases with the stroke ratio when $L_m/D_0 \leqslant 2.2$. However, as shown in Fig. 7, there is not a significant increase on the vortex diameter with the stroke ratio, i.e. all data overlap for $L_m/D_0 \geqslant 4$. This indicates that the vortex ring reaches a limit size even though the stroke (piston displacement) keeps on increasing. Gharib et al. [10] pointed out this constraint in their experimental results for Newtonian vortex rings. Previous investigations [9,11] show that the diameter of Newtonian vortices does not depend on the Reynolds numbers. However, as seen in Fig. 6a the diameter $D_v = 2r$ changes with Re_0 for a given shear-thinning fluid; besides, for the same Re_0 but different n (Fig. 6b) the evolution of the vortex trajectory, and therefore the vortex diameter is different.

Fig. 8 shows the axial velocity profiles u_x that the vortices produce along the axial axis ($r = 0$): (a) the ST1 fluid for $Re_0 = 616$ and

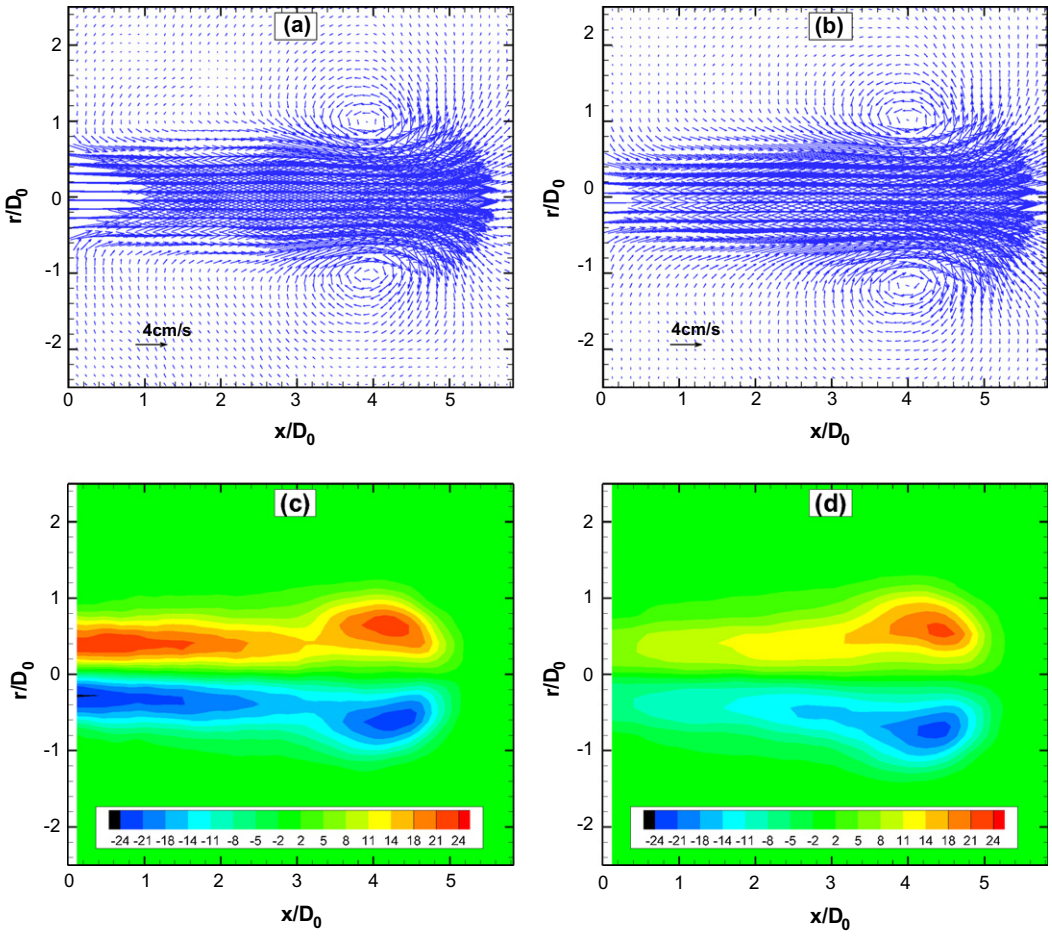

Fig. 5. Comparison of vector and vorticity fields for N and ST3 fluids. $L_m/D_0 = 8$, $Re_0 = 260$ and $x = 4D_0$.

(b) all liquids for $Re_0 \approx 260$ and a stroke ratio of $L_m/D_0 = 4$. Each curve represents the profile of a single vortex ring and the vortex center is located at $x \approx 4D_0$. We can observe that the maximum axial velocity values coincide well with the vortex ring center position. Fig. 8a shows that the value of the velocity profile u_x increases with the stroke ratio. For small stroke ratios we observe that the u_x-velocity profile is symmetric, while for $L_m/D_0 \geqslant 4$ a trailing jet flow connected with the leading vortex is observed. As will be discussed later in this paper, the axial velocity (at $r = 0$) inside the cylinder is actually larger than the mean piston velocity. The above can be observed in the velocity profile of $L_m/D_0 = 10$ for which the piston is still moving and the velocity at the nozzle exit is $u_x(x = 0, r = 0)/U_p \approx 1.2$. Fig. 8b shows the horizontal velocity profile for all liquids with $Re_0 \approx 260$ and $L_m/D_0 = 4$. We observe clearly that when increasing the thinning property (decreasing n) of the fluid, the velocity profiles values decrease too. The velocity profile from the Newtonian case has the largest values. We will also explain this further in the discussion section.

Fig. 9 shows the non-dimensional propagation velocity U_v of vortex rings; again considering the ST1 fluid first ($L_m/D_0 = 8$) for different Reynolds number (Fig. 9a); and then, keeping the Reynolds and stroke ratio fixed, varying only the thinning property of the liquid (varying n) in Fig. 9b. The propagation velocity is obtained by the numerical differentiation of the center position of single vortex rings. In Fig. 6a we observe that the initial velocity is in the range $0.4 \leqslant U_v/U_p \leqslant 0.5$ for the three Re_0. The maximum vortex velocity ($\sim 0.6U_p$) is reached at $x \approx 3D_0$; beyond this distance the vortex propagation velocity remains constant for $Re_0 = 265$ and $Re_0 = 616$, but a reduction of velocity is expected at farther distances. For the lower Reynolds number the vortex ring velocity decays faster, as was expected. Fig. 9b shows the propagation velocity of vortex rings for all the liquids with $Re = 260$ and $L_m/D_0 = 4$. The initial velocity also lays in the range $0.4 \leqslant U_v/U_p \leqslant 0.5$. It is interesting to note that the vortex propagation decreases with the thinning property of the liquid. For the Newtonian case the propagation velocity is the highest. This graph is consistent with Fig. 8b where we observe that the axial velocity u_x decreases with the thinning property. Didden [9] and Weigand and Gharib [11] showed that the vortex ring velocity decays with time. For an inviscid fluid, Mohseni and Gharib [16] predicted analytically a propagation velocity of $U_v = 0.5U_p$ while Linden and Turner [21] also predicted a maximum propagation velocity of $U_v \approx 0.7U_p$ for a Norbury [33] family of vortex rings. Querzoli et al. [13] reported experimental results of the propagation velocity and obtained maximum velocities in the range $0.6 \leqslant U_v/u_*(t) \leqslant 0.8$ where $u_*(t)$ is the integrated velocity over the discharged time. Compared with different data reported in the literature, for Newtonian vortices and $Re_0 \sim$ O(1000), the vortex velocity decays faster because viscous dissipation.

3.3. Vortex circulation

Fig. 10 shows the non-dimensional vortex ring circulation as a function of the distance x/D_0, considering again the two comparison used in Figs. 6, 8 and 9. In the present investigation, we used the Q criterion to compute the vortex ring circulation. The vortex circulation is obtained by

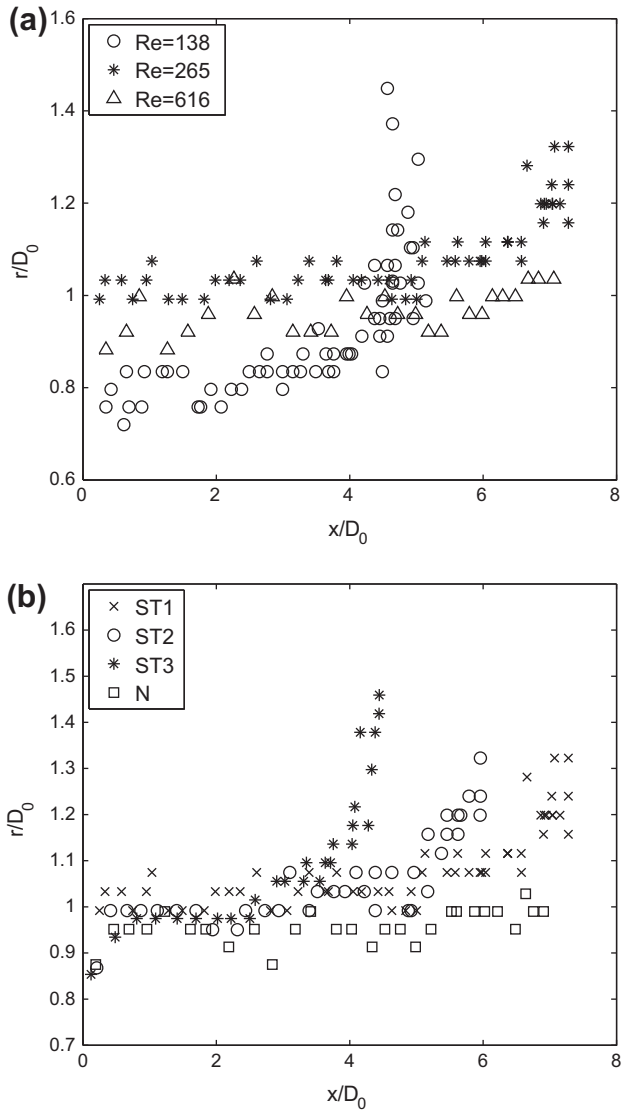

Fig. 6. Trajectories of vortices (maximum curvature). (a) ST1 fluid, $L_m/D_0 = 4$, for different Reynolds. (b) All liquids for $Re_0 \approx 260$ $L_m/D_0 = 4$.

$$\Gamma = \int_{A_Q} \omega_\phi \, dA \tag{9}$$

where ω_ϕ is the azimuthal vorticity (normal to the measurement plane) and A_Q is the region of flow where $Q > 0$ (for our calculations we consider $Q \geqslant 0.01 s^{-2}$). Querzoli *et al.* [13] used the Δ criterion proposed by Chong et al. [26] to identify the vortex ring area on the measurement plane. Note that considering this method to measure the circulation, only the vorticity in the core of the vortex is considered. The points plotted in Fig. 10 (and all data with error bars presented in this paper) correspond to the average of five different runs of the piston and the error bars represent the standard deviation. It is important to note that for all the non-Newtonian fluids studied in the present investigation, we did not observe a 'physical separation' between the leading vortex ring and its trailing jet for large stroke ratios.

In Fig. 10a, we present the vortex circulation for the ST3 fluid at a fixed Re_0 and different stroke ratios. For low stroke ratios $L_m/D_0 \leqslant 4$ we observed that the vortex circulation decreases as soon as the vortex ring is formed. For larger stroke ratios the vortex circulation first increases, reaches a maximum value and beyond a certain distance x/D_0 from the the exit, it decreases. This means

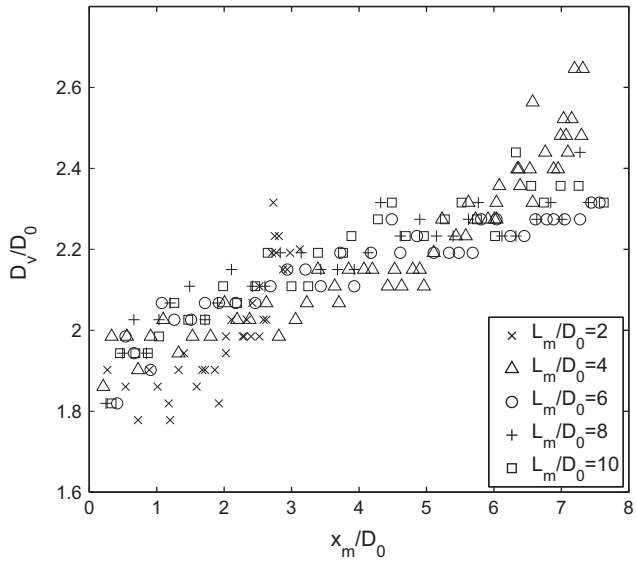

Fig. 7. Vortex ring diameters for the ST1 liquid with $Re_0 = 265$.

that the vortex ring is initially fed of vorticity until it gets a saturation condition for which is not possible to attain more vorticity in its core; after some time, the vorticity in the vortex is dissipated. These features are similar to those observed for Newtonian liquids; the distance for which the vortex circulation decays depends on the stroke ratio and, in general, on the Reynolds number [15]. In Fig. 10b we present the vortex circulation for all the liquids presented in previous sections for a stroke ratio $L_m/D_0 = 8$. The Reynolds number is the same in all cases. We observe that, at any distance, the circulation value is slightly larger for liquids with larger n. In other words, the vortex circulation decreases as the fluids become more shear-thinning. Similarly, the vortex circulation first increases, reaches a maximum value and finally decreases. It is interesting to note that the trend for all liquids is similar.

Fig. 11 shows the non-dimensional vortex ring circulation as a function of the stroke ratio L_m/D_0 for the ST1 liquid with $Re_0 = 265$. Each data series corresponds to different vortex ring positions x/D_0. As expected, the maximum vortex ring circulation for each stroke ratio is reached at different distances of measurement; similar results have been reported by Rosenfeld et al. [15] for Newtonian vortex rings. Fig. 11 shows that the maximum values of vortex ring circulation for $L_m/D_0 \leqslant 3$ occur at a distance close to $x/D_0 = 1$ which is markedly close to the exit. For larger stroke ratios the maximum circulation is reached farther. For Newtonian vortex rings and Reynolds numbers of O(1000), Gharib et al. [12] presented maximum values of vortex circulation at a distance close to $x = 10D_0$. We also observe that all the vortex ring circulation values in this case and for larger Reynolds numbers, were below the saturation value $\Gamma/D_0U_p \approx 2$. With this information it is possible to obtain the maximum vortex ring circulation for each stroke ratio regardless the position where it is reached.

Fig. 12 shows the maximum vortex circulation for each L_m/D_0 following the comparison scheme described above. In Fig. 12a we observe that for stroke ratios $L_m/D_0 \leqslant 4$ the vortex circulation is larger for lower Reynolds numbers (compare the cases $Re_0 = 138$ and $Re_0 = 616$). For the case $Re_0 = 138$, when $L_m/D_0 \approx 3$, the circulation achieves a maximum value and does not increase significantly, i.e. the vortex ring circulation saturates at this stroke ratio. However, for the other Reynolds numbers, we observe that is possible to further increase the vortex ring circulation. Note that as we increase the strain rate (increasing the piston velocity) for a shear-thinning fluid, the viscosity is reduced at the cylinder wall.

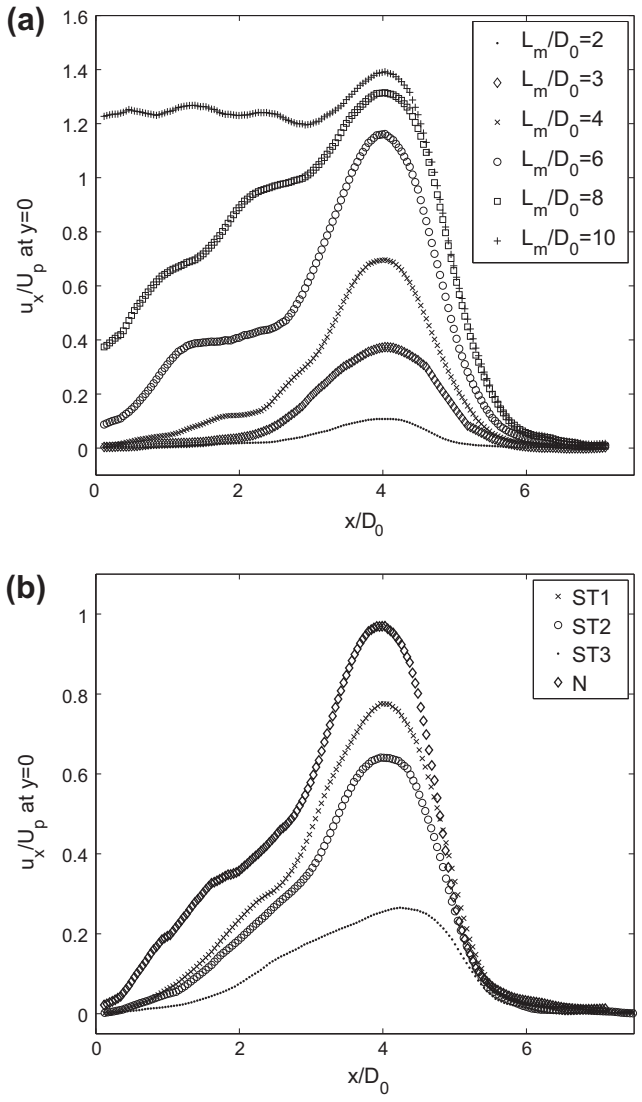

Fig. 8. Axial velocity profile at $r = 0$. (a) ST1 fluid $Re_0 = 616$. (b) Different liquids $Re_0 \approx 260$ and $L_m/D_0 = 4$.

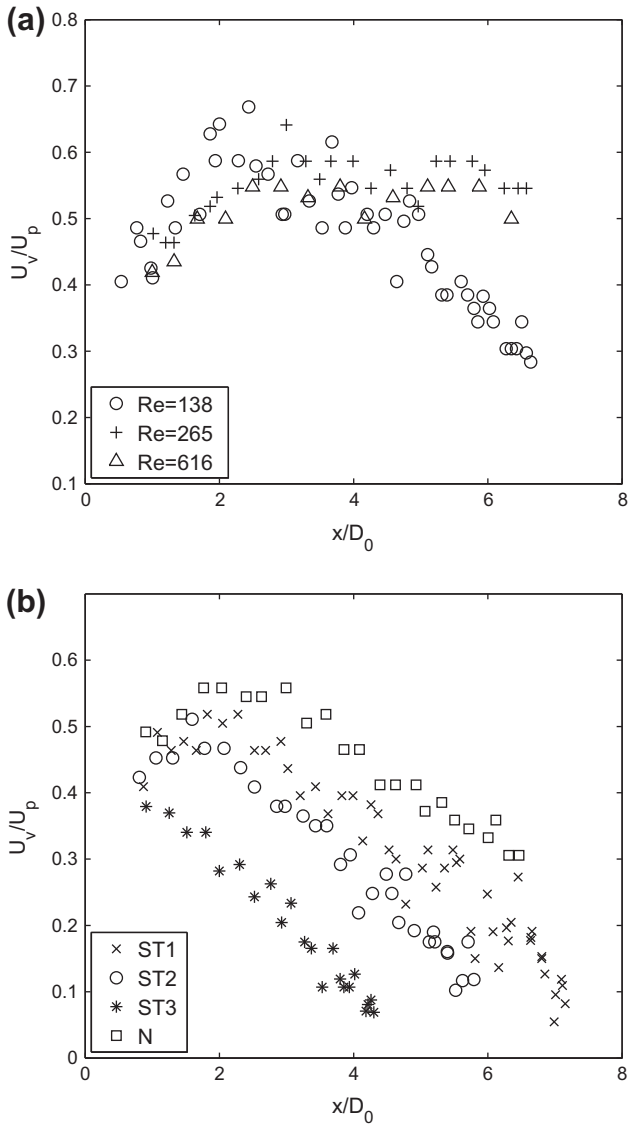

Fig. 9. Propagation velocity of vortex rings. (a) ST1 for different Re_0 and $L_m/D_0 = 8$. (b) Different liquids $Re_0 \approx 260$ and $L_m/D_0 = 4$.

Fig. 12b shows the maximum vortex ring circulation for different liquids (shear thinning and Newtonian). To study the effect of the power index n on the vortex ring circulation, we kept the Reynolds number fixed. Remember that n represents the thinning property of the fluid (as n decreases the fluid becomes more shear thinning). First, we observe that the largest circulation is achieved for the Newtonian fluid ($n = 1$); as the thinning property of the fluid increases (decreasing n) the circulation that the vortex ring can attain is reduced. In other words, the vortex ring circulation decreases with n. It is important to observe that the trend of the curves for all liquids is very similar: the vortex ring circulation increases with the stroke ratio and close to $L_m/D_0 = 6$, we detect a change of slope, which suggest that the vortex has reached a 'saturation' state of formation. This is in accordance to what has been observed for Newtonian vortices for larger Re_0.

4. Discussion

To help explain why the vortex circulation decreases with n, we consider the flow inside a round pipe for a power law fluid. The purpose of this exercise is to gain some insight on the production of vorticity and circulation within the tube which in turn, affects the formation of the vortex ring. Consider the flow through a circular tube with radius R shown in Fig. 13. We assume that the flow is axisymmetric, steady, laminar, incompressible and fully developed; the gravity is negligible and there are isothermal conditions. δ is a given distance from the wall to the tube center $\delta = R - r$. The axial velocity $u_x = u_x(r)$, $u_\theta = 0$ and $u_r = 0$. The standard solution for a pipe flow of a power-law liquid gives [34]:

$$u_x = \frac{n}{n+1}\left(\frac{G}{2m}\right)^{1/n}\left[R^{(n+1)/n} - r^{(n+1)/n}\right] \tag{10}$$

where the pressure gradient $G = -\partial p/\partial x$ = constant. The flow rate can be determined by integrating the velocity profile

$$Q = \frac{\pi R^3}{1/n+3}\left(\frac{GR}{2m}\right)^{1/n} \tag{11}$$

Observe that for $n = 1$ and $m = \mu$, we recover the Newtonian case of a Poiseuille flow from Eqs. (10) and (11). The pressure gradient G can be interpreted as the constant force acting over the volume of fluid to conserve the flow rate Q constant. This force is that acting

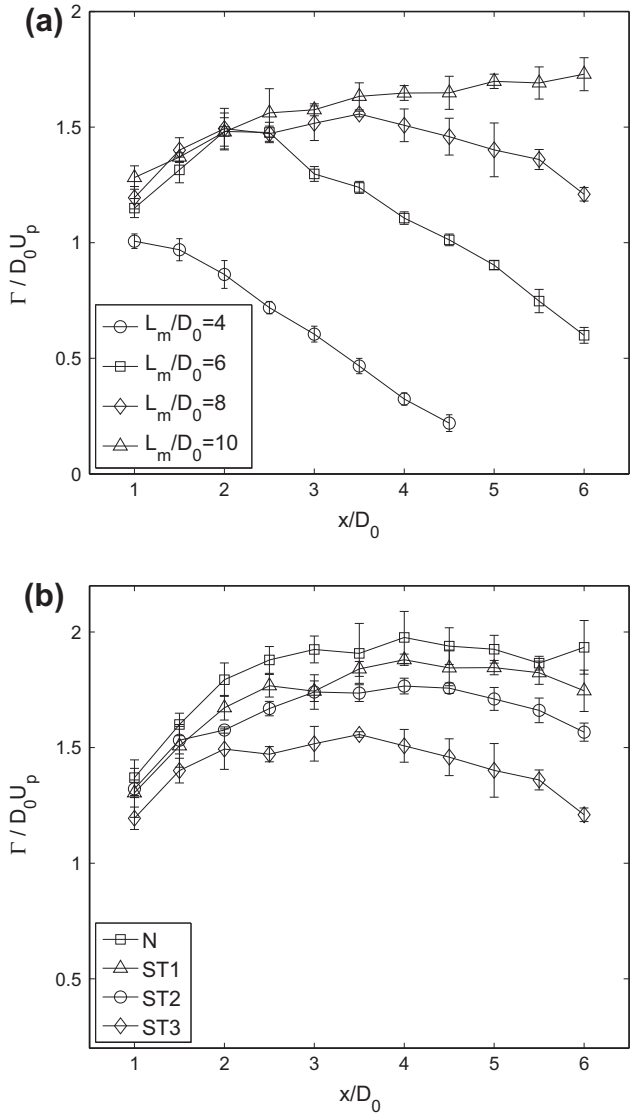

Fig. 10. Non-dimensional vortex ring circulation as a function of the distance x/D_0. (a) ST3 $Re_0 = 262$. (b) Different liquids with $Re_0 \approx 260$ and $L_m/D_0 = 8$.

over the piston that displaces the fluid. The actual flow rate can be determined considering the volume of fluid discharged through the tube exit during a known time:

$$Q = \frac{\pi R^2 L_m}{T_0} \tag{12}$$

For an impulsive velocity program $Q = \pi R^2 U_p$. Substituting expression (12) in Eq. (11), we obtain an effective value of G:

$$G = \frac{2m}{R}\left[\left(\frac{U_p}{R}\right)\left(\frac{1}{n}+3\right)\right]^n \tag{13}$$

Considering the properties of the liquids presented in Table 1, we can compute the axial velocity profile using Eqs. (10) and (13). The velocity profiles are presented in Fig. 14 for all the liquids considered experimentally for a Reynolds number $Re_0 \approx 260$. For all cases the maximum velocity value is located at the center of the tube. For the Newtonian fluid ($n = 1$) we observe a parabolic profile while a more plug-like velocity profile is observed as n decreases; i.e. the axial velocity at the tube center becomes flatter. The maximum velocity for the Newtonian fluid is $u_{max} = 2U_p$ while the maximum velocity for the shear-thinning is reduced. However,

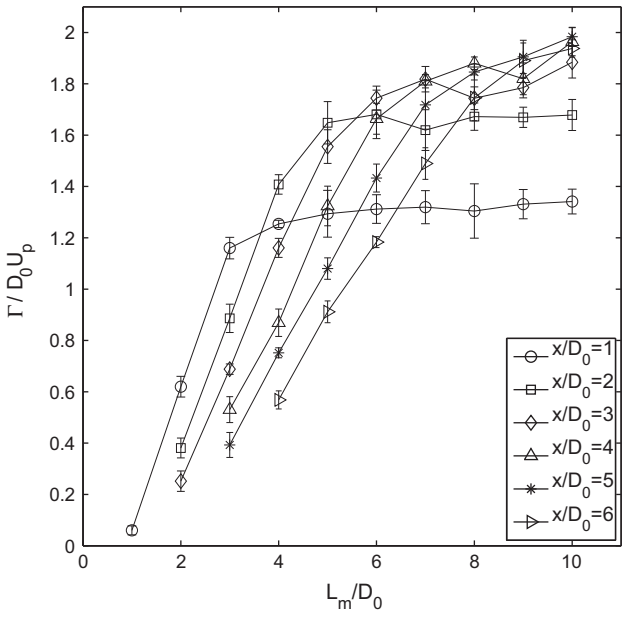

Fig. 11. Non-dimensional vortex ring circulation as a function of L_m/D_0 at different distances for the ST1 fluid and $Re_0 = 265$.

as n decreases, the axial velocity close to the wall can be slightly larger for the shear-thinning fluids than the Newtonian case. This can be explained as follows: the shear rate is larger close to the wall; in this zone, the apparent liquid viscosity for shear-thinning liquids decreases considerably and thus, the liquid flows more easily. The vorticity distribution can also be calculated for this flow:

$$\omega_\phi = -\frac{\partial u_x}{\partial r} = \left(\frac{G}{2m}\right)^{1/n} r^{1/n} \tag{14}$$

In Fig. 15 we show the vorticity distribution for the test liquids at different distances from the tube center. We observe that for all cases, the vorticity value increases as we approach to the wall. For the Newtonian case the dependence with r is linear. It is interesting to note that for the ST1 liquid with $n = 0.61$ (Xan-450 ppm), the vorticity is always lower than the Newtonian case, while for the ST3 liquid the vorticity increases considerably close to the wall. The vorticity close to the tube center is larger for the Newtonian liquid.

Finally, we can use the 'slug' approximation model (described in Section 1.1) to determine the circulation ejected through nozzle. The circulation was defined in Eq. (4); integrating the vorticity over a distance δ from the tube wall we have:

$$\Gamma = \int_0^{T_0} \left[-\frac{u_x^2}{2}\right]_{R-\delta}^{R} dt \tag{15}$$

hence, we obtain

$$\Gamma_T = \frac{n^2}{2(n+1)^2}\left(\frac{G}{2m}\right)^{2/n}\left[R^{(n+1)/n} - (R-\delta)^{(n+1)/n}\right]^2 \frac{L_m}{U_p} \tag{16}$$

With this formula we can obtain the total circulation produced within the tube during the piston displacement. This circulation will, then, be ejected through the nozzle to form the vortex ring (and a trailing jet for large L_m/D_0). Note that the only unknown variable is δ. In Fig. 16 we show the total circulation as a function of δ for a stroke ratio of $L_m/D_0 = 5$. We consider this value to make sure that only a single vortex is generated. For small δ the total circulation is slightly larger as n decreases; the circulation for the Newtonian liquid is the lowest. For δ close to 1, the total circulation is

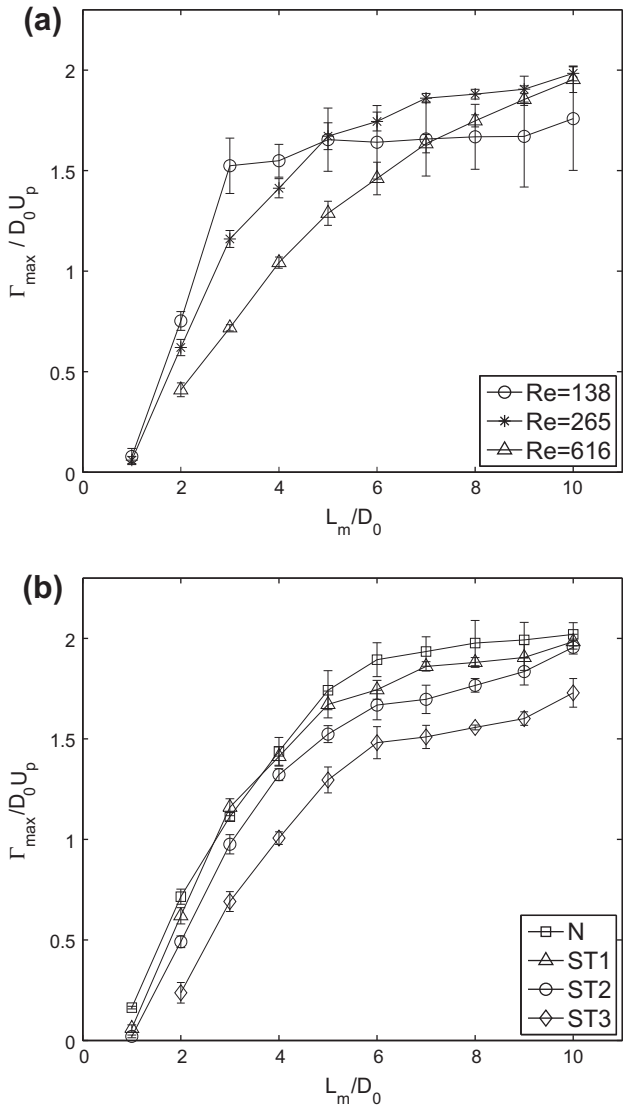

Fig. 12. Maximum vortex ring circulation as a function of L_m/D_0. (a) ST1 fluid. (b) All liquids for $Re_0 \approx 260$.

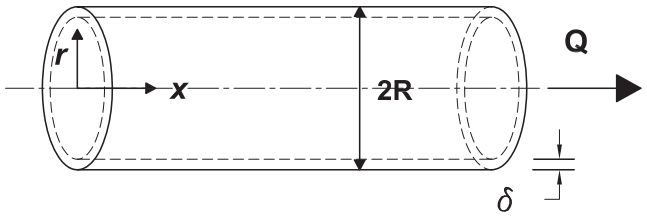

Fig. 13. Flow through a circular tube.

larger as n increases; the circulation for the Newtonian liquid case is notably larger than the others as $\delta \to R$. Note that this calculation considers the same Reynolds number for all liquids. There is a critical δ value where all shear thinning curves coincide the Newtonian curve. This point is located at different δ for each liquid, but it is always close to $\delta \approx 0.45R$. When δ has this value the total circulation values are approximately the same for all liquids for any L_m/D_0.

The question is, how large should the distance δ be for a given liquid?. The slug approximation for Newtonian vortices described

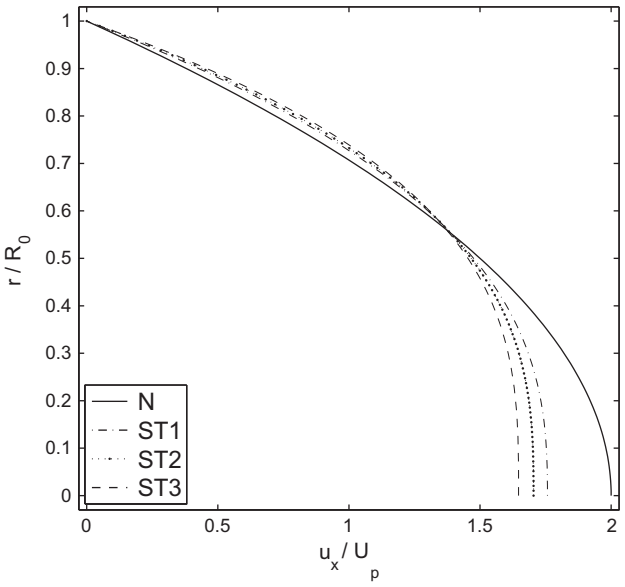

Fig. 14. Axial velocity profile for the flow of a shear-thinning liquid in a circular pipe for the test liquids used in the present investigations, $Re_0 \approx 260$ (considering the properties listed in Table 1).

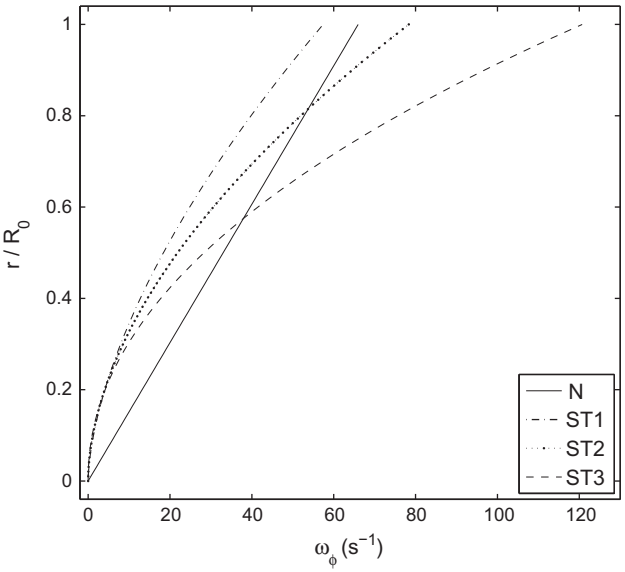

Fig. 15. Vorticity distribution for the test liquids.

before, assumes that a boundary layer forms near the wall ($\beta \ll R$) and the velocity at the edge of the boundary is equal to the piston velocity U_p. This is correct only when the Re_0 is sufficiently large. As the Reynolds number decreases, this approximation becomes incorrect. From the velocity profiles shown in Fig. 14b we can see that for this particular Reynolds number the boundary layer is not thin. Therefore, the calculation of the circulation considering small values of δ is not the most appropriate. Didden [9] also reported that at large discharge times, boundary layer grows leading to an increment in the velocity at the center of the cylinder in order to satisfy continuity. From our calculations, the velocity at the center is $u_x|_{r=0} > 1.5U_p$ which is in agreement with the discussion of Didden [9].

These arguments suggest that δ might be as large as the pipe radius. In Fig. 17 we show the total circulation as a function of L_m/D_0

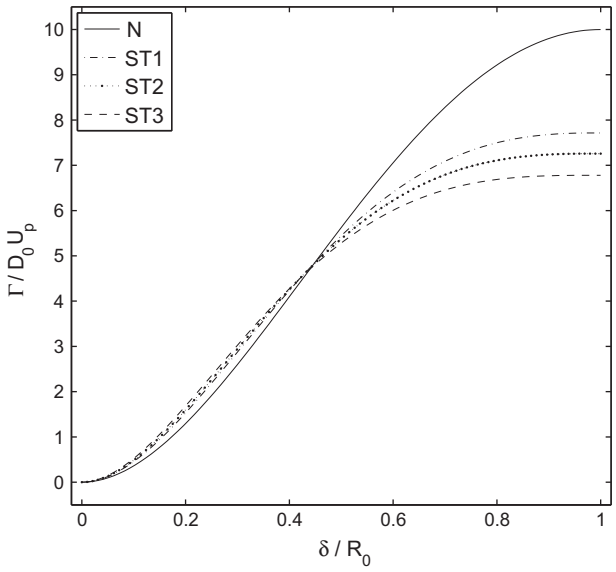

Fig. 16. Total circulation as a function of δ for the test liquids; $L_m/D_0 = 5$.

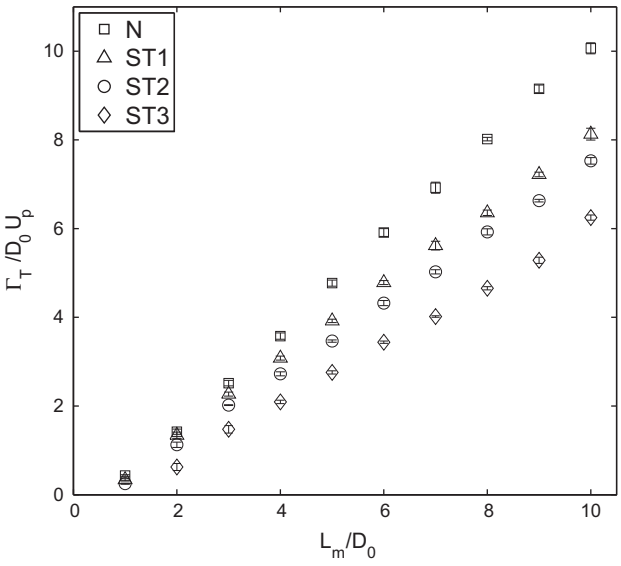

Fig. 18. Experimental total circulation as a function of L_m/D_0 for the test liquids.

for all liquids and $\delta = R$. The total circulation increases linearly, but the slope decreases with n. The total circulation ejected from the tube is reduced as n decreases for all the stroke ratios.

In Fig. 18 we show total circulation for the test liquids obtained from the experiments. The total circulation is determined by integrating the vorticity $\omega_\phi > 0$ in the entire visible domain. The average of five different runs of the piston is plotted with its standard deviation (error bars). Similar to the vortex circulation, the total circulation changes with time; therefore, we plot the maximum circulation value for each L_m/D_0. We observe that the total circulation increases with the stroke ratio and is the largest for the Newtonian case. As n decreases the total circulation decreases too. These experimental results are in agreement with the results presented if Fig. 17 for which $\delta = R$. Although the trend predicted by our model is in agreement with that found experimentally, the quantitative comparison reveals that the predicted circulation is about twice the experimental value. This difference might be explained by different factors. First, at the beginning of the piston movement the flow inside the tube is not fully developed; thus our calculated vorticity is over-predicted. For low Reynolds numbers, vorticity dissipation is important: as the jet of fluid is expelled from the nozzle and the vortex ring is forming, circulation is lost by vorticity dissipation at the axis of symmetry.

Despite these differences, the simple model give us the correct trend and explains why the circulation attained by a vortex ring decreases with the thinning nature of the fluid.

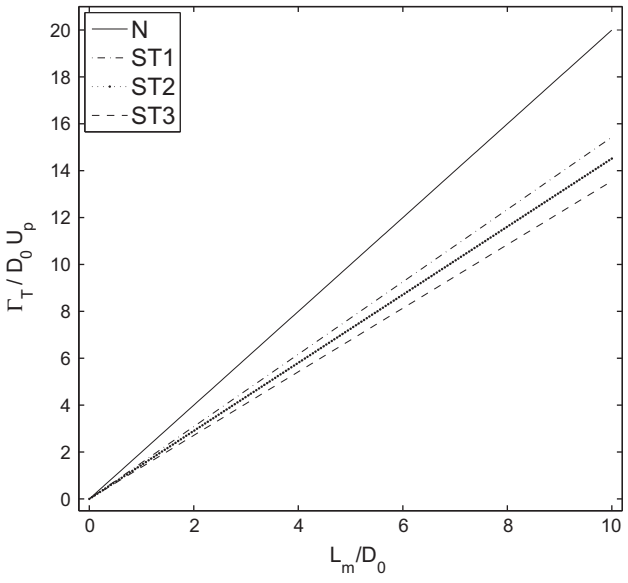

Fig. 17. Total circulation as a function of L_m/D_0 for the test liquids $\delta = R$.

5. Conclusions

The experimental results presented in this paper indicate that the vortex ring circulation decreases with n. We have derived a formula to obtain the total circulation ejected from a cylinder tube considering the slug model and the solution for a pipe flow of a power-law liquid. We have shown that the total circulation ejected from the tube is reduced as the thinning property increases; thus, the circulation confined inside the vortex is reduced too. The trend predicted by our model is in agreement with the experimental results; however, the circulation values are over predicted by a factor of about 2. We also observed that the initial size (diameter) of the vortex ring does not depend on the rheological properties of the fluid; however, shear-thinning vortices expands in the radial direction after some discharge time for low stroke ratios. The measurements of the vortex propagation velocity for the same Reynolds number, indicate that the travel velocity is reduced with the thinning property (decreasing n) of the fluid.

It is important to note that as we increase the thinning nature of the fluid (decreasing n) the consistency m also increases. In regions of flow where the local velocity is low (low shear strain) the apparent viscosity increases considerably. Hence, slow moving fluid surrounding the moving vortex rings will have a larger viscosity. Therefore, we can expect the vortex ring propagation velocity to be smaller and to decrease quickly as n decreases.

All the non-Newtonian vortex rings studied in this investigation have relatively small Reynolds numbers; hence, it was not possible to observe a 'physical separation' between the leading vortex ring and its trailing jet. Some authors have stated that there is not vortex ring pinch-off if it is not possible to guarantee the mentioned separation. Therefore, it is difficult to study a vortex ring formation number as defined by Gharib et al. [12]. However, we observe that the vortex ring circulation increases with the stroke ratio L_m/D_0

until it reaches a 'saturation state' close to $L_m/D_0 = 6$ where we detect a change of the slope. This suggests that the vortex ring cannot attain vorticity in the same rate as L_m/D_0 increases. This observation is valid for Newtonian and shear thinning fluids; however, the maximum circulation that a vortex can attain is reduced as the liquid becomes more shear-thinning.

Acknowledgements

The financial support from CONACYT-México (Grant No. 102927) is greatly appreciated. We are also grateful to the Dirección General de Estudios de Posgrado (DGEP-UNAM) for granting C.P.-M. a doctorate scholarship.

References

[1] E.J. Anderson, M.A. Grosenbaugh, Jet flow in steadily swimming adult squid, J. Exp. Biol. 208 (2005) 1125–1146.
[2] I.K. Bartol, P.S. Krueger, W.J. Stewart, J.T. Thompson, Pulsed jet dynamics of squid hatchlings at intermediate Reynolds numbers, J. Exp. Biol. 212 (2009) 1506–1518.
[3] J.O. Dabiri, S.P. Colin, J.H. Costello, Fast-swimming hydromedusae exploit velar kinematics to form an optimal vortex wake, J. Exp. Biol. 209 (2006) 2025–2033.
[4] M. Gharib, E. Rambod, A. Kheradvar, D.J. Sahn, Optimal vortex formation as an index of cardiac health, Proc. Natl. Adad. Sci. USA 103 (2006) 6305–6308.
[5] K. Shariff, A. Leonard, Vortex rings, Ann. Rev. Fluid Mech. 24 (1992) 235–279.
[6] T.T. Lim, T.B. Nickels, Vortex rings, in: S.I. Green (Ed.), Fluid Vortices, Kluwer Academic Publisher, 1995, pp. 95–153.
[7] P.G. Saffman, Vortex Dynamics, Cambridge Univ. Press, 1992.
[8] T. Maxworthy, Some experimental studies of vortex rings, J. Fluid Mech. 81 (1977) 465–495.
[9] N. Didden, On the formation of vortex rings: rolling-up and production of circulation, Z. Angew. Mech. Phys. 30 (1979) 101–116.
[10] A. Glezer, The formation of vortex rings, Phys. Fluids 31 (1988) 3532–3542.
[11] A. Weigand, M. Gharib, On the evolution of laminar vortex rings, Exp. Fluids 22 (1997) 447–457.
[12] M. Gharib, E. Rambod, K. Shariff, A universal time scale for vortex ring formation, J. Fluid Mech. 360 (1998) 121–140.
[13] G. Querzoli, M. Falchi, G.P. Romano, On the flow field generated by a gradually varying flow through an orifice, Eur. J. Mech. B – Fluid. 29 (2010) 259–268.
[14] C. Palacios-Morales, R. Zenit, Vortex ring formation for low Re numbers, Acta Mech. in press, http://dx.doi.org/10.1007/s00707-012-0755-4.
[15] M. Rosenfeld, E. Rambod, M. Gharib, Circulation and formation number of laminar vortex rings, J. Fluid Mech. 376 (1998) 297–318.
[16] K. Mohseni, H. Ran, T. Colonius, Numerical experiments on vortex ring formation, J. Fluid Mech. 430 (2001) 267–282.
[17] P.M. Coelho, F.T. Pinho, Vortex shedding in cylinder flow of shear-thinning fluids I. Identification and demarcation of flow regimes, J. Non-Newtonian Fluid Mech. 110 (2003) 143–176.
[18] P.M. Coelho, F.T. Pinho, Vortex shedding in cylinder flow of shear-thinning fluids II. Flow characteristics, J. Non-Newtonian Fluid Mech. 110 (2003) 177–193.
[19] G. Bohme, L. Rubart, M. Stenger, Vortex breakdown in shear-thinning liquids: experiment and numerical simulation, J. Non-Newtonian Fluid Mech. 45 (1992) 1–20.
[20] K. Mohseni, M. Gharib, A model for universal time scale of vortex ring formation, Phys. Fluids 10 (1998) 2436–2438.
[21] P.F. Linden, J.S. Turner, The formation of optimal vortex rings, and the efficiency of propulsion devices, J. Fluid Mech. 427 (2001) 61–72.
[22] J.C.R. Hunt, A. Wray, P. Moin, Eddies, Stream, and Convergence Zones in Turbulent Flows, Center for Turbulence Research Report CTR-S88, 1988.
[23] A. Okubo, Horizontal dispersion of floatable trajectories in the vicinity of velocity singularities such as convergencies, Deep-Sea. Res. 17 (1970) 445–454.
[24] J. Weiss, The dynamics of enstrophy transfer in 2-dimensional hydrodynamics, Physica D 48 (1991) 273–294.
[25] N.T. Oullette, J.P. Gollub, Curvature fields, topology, and the dynamics of spatiotemporal chaos, Phys. Rev. Lett. 99 (194502) (2007).
[26] M.S. Chong, A.E. Perry, B.J. Cantwell, A general classification of three-dimensional flow fields, Phys. Fluids A 2 (1990) 765–777.
[27] W. Braun, F. de Lillo, B. Eckhardt, Geometry of particle paths in turbulent flows, J. Turbul. 7 (62) (2006).
[28] H.A. Barnes, J.F. Hutton, K. Walters, An Introduction to Rheology, Elsevier, 1989.
[29] C. Willert, M. Gharib, Digital particle image velocimetry, Exp. Fluids 10 (1991) 181–193.
[30] M. Raffel, C. Willert, J. Kompenhans, Particle Image Velocimetry. A Practical Guide, Springer, 1998.
[31] N. Benard, S. Jarny, D. Coisne, Definition of an experimental blood like fluid for laser measurements in cardiovascular studies, Appl. Rheol. 17 (2007) 44251-1–44251-8.
[32] J.R. Vélez-Cordero, D. Sámano, P. Yue, J.J. Feng, R. Zenit, Hydrodynamic interaction between a pair of bubbles ascending in shear-thinning inelastic fluids, J. Non-Newtonian Fluid Mech. 166 (2011) 118–132.
[33] J. Norbury, A family of steady vortex rings, J. Fluid Mech. 57 (1973) 417–431.
[34] F.A. Morrison, Understanding Rheology, Oxford University Press, 2001.